Geophysical Journal International

Geophys. J. Int. (2012) **191,** 707–722 doi: 10.1111/j.1365-246X.2012.05638.x

Modelling long-term seismic noise in various environments

E. Stutzmann,[1] F. Ardhuin,[2] M. Schimmel,[3] A. Mangeney[4] and G. Patau[1]

[1] *Institut de Physique du Globe de Paris, Sorbonne-Paris-Cité, Paris, France. E-mail: stutz@ipgp.fr*
[2] *Laboratoire d'Océanographie Spatiale, Ifremer, Plouzané, France*
[3] *Institute of Earth Sciences Jaume Almera, CSIC, Barcelona, Spain*
[4] *Institut de Physique du Globe de Paris, Université Paris Diderot, Sorbonne-Paris-Cité, Paris, France*

Accepted 2012 July 27. Received 2012 July 27; in original form 2011 April 7

SUMMARY

The strongest seismic noise, called secondary microseisms, is generated by ocean wave interactions and we model this noise using the theory of Longuet-Higgins generalized to random ocean gravity waves. Noise sources are computed with an ocean wave model that takes into account coastal reflections. Variations of the source locations are consistent with seasonal variations of seismic noise spectra. Noise spectra are modelled over many years for stations representative of various environments such as continent, island and polar area to constrain, for each environment, the parameters involved in the modelling. For each station, we quantify the trade-off between ocean wave coastal reflection and seismic wave attenuation that both affect the amplitude of the seismic spectrum. We show their adjustment and the need, at some stations, for an extra parameter representing the three-dimensional (3-D) seismic wave propagation effects. The long-term analysis demonstrates the stability of the fitted parameters which can be used in future noise studies. The modelling enables to reproduce the frequency content and amplitude of the different noise peaks of seismic spectra. The strongest peaks are generated by deep ocean sources whereas coastal reflections generate numerous smaller sources that contribute to the background noise level. Coastal reflection effects can be neglected only for the Pacific island station PPT. The modelling also reproduces the peculiar noise spectrum variation in Antarctica (station DRV) which is related to the presence of sea ice around the stations.

Key words: Surface waves and free oscillations; Theoretical seismology; Wave propagation.

1 INTRODUCTION

In the absence of earthquakes, seismic noise called microseisms is omnipresent and clearly visible on seismograms recorded by broadband stations whatever their locations, on continents, on islands (e.g. Peterson 1993; Stutzmann *et al.* 2000) or on the ocean bottom (Montagner *et al.* 1994; Webb 1998; Stutzmann *et al.* 2001). Microseisms are observable in the frequencies band 0.05–0.2 Hz. Their spectra are characterized by two peaks around 0.07 and 0.014 Hz, which correspond to the so-called primary and secondary microseisms. Secondary microseisms are dominantly Rayleigh waves (e.g. Haubrich & McCamy 1969) and have the strongest amplitude. The primary microseisms have smaller amplitude and the corresponding energy ratio between Love wave and Rayleigh waves is about 1.2 (Friedrich *et al.* 1998; Nishida *et al.* 2008).

Relationships between storms, ocean waves and microseisms have been reported by many authors since the 19th century (Bernard 1990). The primary microseisms (frequencies around 0.07 Hz) are generated when ocean waves reach shallow water near the coast and interact with the sloping seafloor (Hasselmann 1963). The seismic waves have the same frequencies as the incident ocean gravity waves. The secondary microseisms (strongest frequencies between 0.1 and 0.2 Hz) are generated by the interaction of ocean waves of similar frequencies that travel in opposite directions. The theory was first proposed by Longuet-Higgins (1950) and then extended to random ocean wave fields by Hasselmann (1963) who expressed the source of seismic noise as a function of the directional wave spectrum. Ocean waves are attenuated exponentially with depth, so they do not reach the ocean bottom in deep water but to the second order, any pair of ocean wave trains can combine to produce pressure fluctuations with a frequency and wave number that is the sum or the difference of those of the wave trains. For wave trains with nearly opposite directions and equal frequencies, the resulting second-order pressure fluctuation has the double of the ocean wave frequencies, and it reaches the ocean bottom. This pressure fluctuation is at the origin of the secondary microseisms by coupling with the ocean bottom. Using asymptotic development taking into account the non-linear effect of wave interference in a compressible ocean, Longuet-Higgins (1950) estimated the expected amplitude of seismic noise. Considering typical values for the oceanic waves

and Earth characteristics, he suggested that microseisms generated in deep ocean should be of higher amplitude than those generated by coastal reflection. Sixty years later, the relative importance of deep ocean and coastal sources is still under debate. Using seismic arrays, Haubrich & McCamy (1969) showed the existence of both coastal and pelagic sources of secondary microseisms. Similar observations were obtained later by Friedrich *et al.* (1998) and Chevrot *et al.* (2007). Over the years, there has been an increasing number of observations of noise sources in the deep ocean (Webb & S.C. 1986; Cessaro 1994; Stehly *et al.* 2006; Kedar *et al.* 2008) and in the near-coastal area (Bromirski & Duennebier 2002; Schulte-Pelkum *et al.* 2004; Rhie & Romanowicz 2006; Gerstoft & Tanimoto 2007; Yang & Ritzwoller 2008). Modelling seismic noise, as presented in this paper, is a unique tool for identifying in seismic noise records, which signal is generated by coastal and/or deep ocean sources.

Seismic noise is mainly used for imaging and monitoring the Earth based on the fact that Green functions between pairs of stations can be obtained from the stack of their noise cross-correlograms (Shapiro & Campillo 2004). This technique has been extensively used over the last decade for passive imaging at crustal scale (Shapiro *et al.* 2005). Nishida *et al.* (2009) and Schimmel *et al.* (2010) showed that seismic noise can also be used for mantle imaging. Variations of the cross-correlograms over time are used for monitoring volcanoes (Sens-Schonfelder & Wegler 2006; Brenguier *et al.* 2008a) and seismic faults (Wegler & Sens-Schonfelder 2007; Brenguier *et al.* 2008b). The extraction of Green's functions rely on the hypothesis that noise sources are randomly distributed. If this assumption is not met, traveltime or velocity measurements may be incorrect (Tsai 2009). Since most noise tomography and monitoring studies are performed in the period band of the secondary microseism, a better knowledge of the corresponding sources and an accurate modelling of the seismic noise recorded by seismic stations are of particular interest.

Seismic noise also enables to investigate sea state. Bromirski *et al.* (1999) used seismic noise recorded by coastal stations in California to determine the ocean significant wave height which was successfully compared with nearby buoy measurements. Ardhuin *et al.* (2012) further showed in which conditions coastal stations can be used as a proxy for the local significant wave height. More generally, the comparison between observed and modelled seismic noise enables to investigate ocean wave parameters in areas without buoys and the historical seismic data can be used to reconstruct past ocean states (Bernard 1990; Grevemeyer *et al.* 2000).

The introduction of numerical modelling of the seismic noise by Kedar *et al.* (2008) opened a new era in the understanding, analysis and practical use of seismic noise. This type of modelling is also an important tool for testing hypotheses on noise source distributions. Ardhuin *et al.* (2011) improved the modelling using more accurate wind fields and parameterizations for wave evolution, and introducing coastal reflections. They provided an extensive description of the ocean wave model, showed the expected distribution of global seismic noise sources yearly averaged, and discussed the typical sea states that generated noise at four selected seismic stations. A qualitative validation of the model was further proposed by Schimmel *et al.* (2011) who compared azimuths derived from noise polarization analysis and source locations. Modelling noise require the adjustment of at least two parameters: the ocean wave coastal reflection and the seismic attenuation. These parameters are empirically determined and not well constrained. Also their validity for long-term modelling is not known. The purpose here is to determine the parameters involved in the modelling for stations representative of various environments such as continent, island and polar area in both hemispheres. We quantify the trade-off between ocean wave coastal reflection and seismic wave attenuation that both affect the amplitude of the seismic spectrum. We show their adjustments and the need, at some stations, for an extra parameter representing the three-dimensional (3-D) seismic wave propagation effects. Our analysis provides values of these empirical parameters together with their uncertainties. The long term analysis demonstrates the stability of the fitted parameters which can then be used in future noise studies. With these empirical parameters, the modelling enables to reproduce the frequency content and amplitude of the different noise peaks of seismic spectra.

2 SEISMIC NOISE VARIATIONS OVER TWO DECADES

To compare observed and modelled seismic noise variations, we processed continuous data recorded by the global network of broadband seismic stations GEOSCOPE. We computed seismic noise power spectra density (PSD) following the same procedure as in Stutzmann *et al.* (2009) who analysed noise variations over 2 yr. We computed daily seismic noise levels for the 27 stations since the beginning of continuous recording of the BH channel, that is from 1989 to 2010. BH and LH channels were used to compute noise PSD in the period bands 0.1–20 s and 5–1000 s, respectively. The good agreement between both spectra in the period range between 5 and 20 s is one way to validate the instrumental responses. Noise PSD of all GEOSCOPE stations since the beginning of continuous recording are available at the site http://geoscope.ipgp.fr.

Seasonal variations of seismic noise are well known (e.g. Stutzmann *et al.* 2000) and the correlation of high noise with highest wave area was shown by Stutzmann *et al.* (2009) at global scale. Aster *et al.* (2008) further showed the long-term consistency of noise recorded by stations over wide areas. Here we selected stations which record typical noise variations to be representative of continent, island and polar environments in both hemispheres. We further selected stations that have been operational with very few gaps and stable recording over 20 yr and therefore are good candidates for validating our noise spectra modelling.

Fig. 1 shows the noise PSD for the seven selected stations sorted by latitude from North to South. The station locations are shown on Fig. 2. Seasonal variations of the secondary microseisms in the period band (5–10 s) are stable over 20 yr. The noise amplitude is maximum in December and January for the northern hemisphere stations SSB in France and INU in Japan and seasonal variations are less visible for station TAM which is located in the middle of the African continent. Considering a statistical analysis of the noise polarization, Schimmel *et al.* (2011) showed that this station records seismic noise generated in oceans all around Africa, that is North Atlantic, South Atlantic and Indian ocean. Station HYB in India is also in the northern hemisphere but we clearly see a maximum of noise during southern hemisphere winter, in July and August. This is because the entire Indian Ocean follows southern hemisphere dynamics as also observed by Koper & Foy (2008). Station PPT (called PPTF since 2009) in Tahiti, in the southern Pacific ocean shows no seasonal variations and station CAN in Australia displays a maximum of noise amplitude in July-August that is during local winter. The last station DRV, is located on a small island close to Antarctica. Stutzmann *et al.* (2009) showed that the observed decrease of noise during winter can be explained by the presence of sea ice over several hundred of kilometres around the station which prevent the generation of noise sources close to the

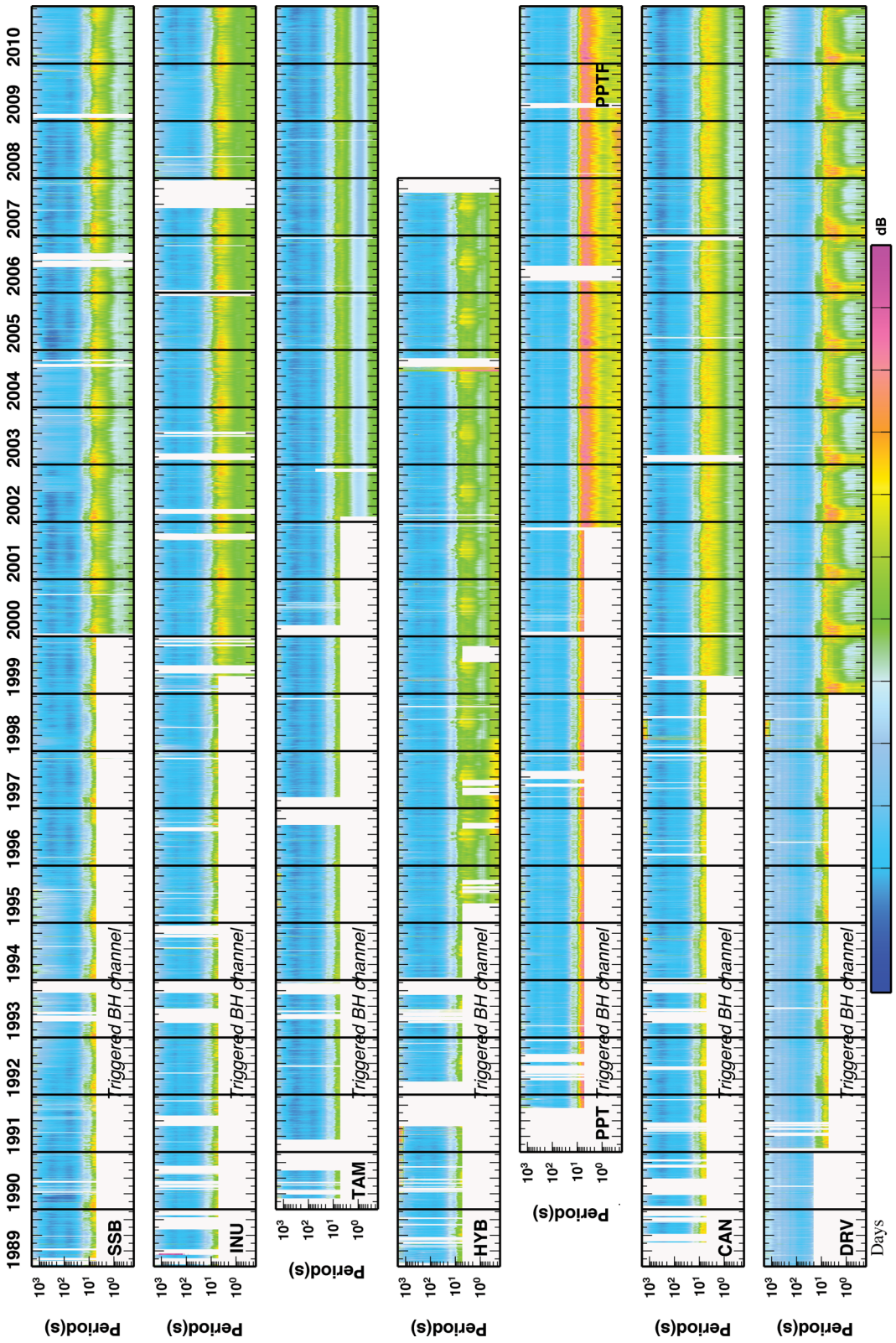

Figure 1. Power spectra density (PSD) of seismic noise from 1989 to 2010 for six stations from the GEOSCOPE global network. Stations are sorted by latitude from north (top panel) to south (bottom panel) and the station names are written on the lower left of each plot. White area correspond to period when data where triggered on earthquake or to missing data. PSD are plotted in dB with respect to acceleration.

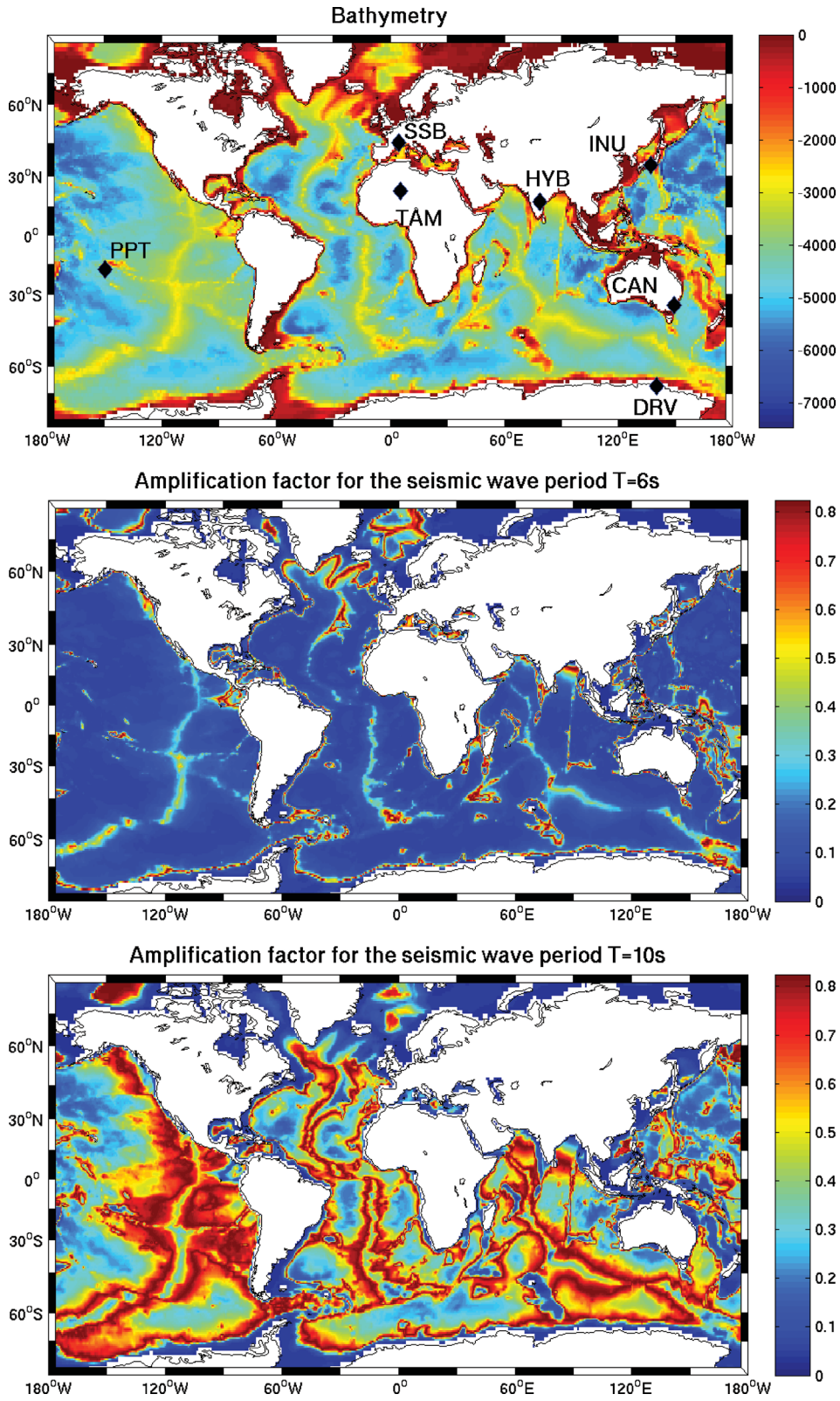

Figure 2. Top panel: station location on the topography map. Middle and bottom panels: amplification factor for the seismic wave period of 6 s and 10 s, respectively.

station. Grob *et al.* (2011) and Tsai & McNamara (2011) observed similar effects for other polar stations in Antarctica and Alaska, respectively. Tsai & McNamara (2011) reproduced the short period ($T = 0.6$–2 s) noise spectra in Alaska by using a station free of ice as a proxy for the short period noise sources which they modulate by the ice concentration. Here we study noise at longer period ($T =$ 3–12 s) and sources are computed from the ocean wave model. In the next sections, we investigate how the modelling can reproduce the observed spectra.

3 THEORY

The theory for modelling seismic noise was proposed during the middle of last century. When two linear ocean gravity wave trains of equal frequency and opposite propagation directions meet, they produce a second-order pressure field that, for an incompressible ocean, is uniform over the water depth (Miche 1944). Longuet-Higgins (1950) introduced the compressibility of water to quantify the generation of seismic waves in a medium composed of a water layer and an elastic half space beneath. Hasselmann (1963) pointed out that the important property for seismic wave generation is that a part of the second-order pressure field has phase velocity matching that of seismic waves. It corresponds to the wave–wave interactions that involve nearly opposing ocean wave trains with nearly equal frequencies. The theory for computing noise synthetic spectra from ocean wave hindcasts can be found in Ardhuin *et al.* (2011) together with the comparison between Hasselmann and Longuet-Higgins theories in the case of monochromatic waves. Hereafter we summarize the theory and we discuss the frequency dependent amplification of the sources and the seismic propagation.

The equivalent pressure spectral power density just below the ocean surface generated by a gravity wavefield can be written following Hasselmann (1963), (eq. 2.15 p. 191),

$$F_p(\mathbf{K} \simeq 0,\, f_2 = 2f) = \rho_w^2 g^2 f_2 \int_0^{\pi} F(f,\theta) F(f,\theta+\pi)\, \mathrm{d}\theta, \quad (1)$$

where ρ_w is the water density, g is the gravity constant, f is the ocean wave frequency. $F_s(f,\, \theta)$ and $F_s(f,\, \theta + \pi)$ are the wave height spectral density for the same frequency f and the two opposite azimuths θ and $\theta + \pi$. These two colliding ocean wave trains generate pressure fluctuations $F_p(\mathbf{K},\, f)$ whose wave number $\mathbf{K}$ is the sum of the wave number of the two opposite ocean waves, (therefore $\mathbf{K} \simeq 0$) and whose frequency is $f_2 = 2f$.

We then define $F(f,\, \theta) = E(f)M(f,\, \theta)$ where $M(f,\, \theta)$ is the non-dimensional ocean wave energy distribution as a function of frequency and azimuth. $E(f)$ is the spectral density of the ocean surface elevation. Eq. (1) can then be rewritten

$$F_p(\mathbf{K} \simeq 0,\, f_2 = 2f) = \rho_w^2 g^2 f_2 E^2(f) \int_0^{\pi} M(f,\theta) M(f,\theta+\pi)\, \mathrm{d}\theta. \quad (2)$$

The integral in eq. (2) is a non-dimensional function that depends on the ocean wave energy spatial distribution. The unit of F_p is $N^2\,\mathrm{m}^{-2}\,\mathrm{Hz}^{-1}$.

Longuet-Higgins (1950) showed that the pressure fluctuations are not attenuated with depth but transmitted to the ocean bottom as acoustic waves. Depending on the ratio between the wavelength of the acoustic waves and the ocean depth, resonance effects can occur leading to a modulation of the pressure fluctuations at the ocean bottom. Then, the corresponding seismic source power spectral density at the ocean bottom is

$$S_{DF}(f_s = f_2) = \frac{2\pi f_s}{\rho_s^2 \beta^5} \left[\sum_{m=1}^{m=N} c_m^2 \right] F_p(\mathbf{K} \simeq 0,\, f_2 = 2f). \quad (3)$$

Eq. (3) is derived from Longuet-Higgins equation (186). S_{DF} is in $\mathrm{m\,Hz}^{-1}$. ρ_s and β are respectively the density and S-wave velocity in the crust. f_s is the seismic frequency which is equal to the pressure fluctuation frequency f_2 and it is the double of the ocean wave frequency f. Coefficients c_m correspond to the compressible ocean amplification factor. c_m are non-dimensional numbers which vary between 0 and 1 as a function of the ratio $2\pi f_2 h/\beta$ where h is the water depth (Longuet-Higgins 1950). Considering the crustal density $\rho_s = 2600\,\mathrm{kg\,m}^{-3}$ and S-wave velocity $\beta = 2800\,\mathrm{m\,s}^{-1}$, Fig. 2 shows the ocean amplification factor $\sum_{m=1}^{m=N} c_m^2$ due to bathymetry for seismic wave periods of 6 and 10 s. For the period of 6 s, the amplification is maximum (0.82) when the water depth is 2272 m, it is equal to 0.06 for a shallow water depth of 500 m, and to 0.09 for a water depth of 6000 m. As a consequence, noise sources in the vicinity of ridges or at a few hundred kilometres from the coast are amplified by a factor 10 or more with respect to sources in deep ocean basin or closer to the coast. For the longer period of 10 s, the high amplification area is much broader, it covers most of the oceans and the maximum amplification is observed for water depth of 3790 m.

The source S_{DF} (eq. 3) excites all types of seismic waves, that is surface waves and body waves of frequency $f_s = f_2$. In the following, we only consider Rayleigh waves which are the most energetic seismic waves recorded by the vertical component of seismometers. The ocean is discretized on a grid and each source S_{DF} located at the colatitude–longitude grid point (ϕ', λ') generates Rayleigh waves which propagate along the Earth surface to the station at the group velocity $U(f_s)$. For a given station located at colatitude ϕ and longitude λ, the power spectrum of the vertical ground displacement is the sum over all grid points to consider the contribution of all sources. Taking into account the geometrical spreading and the seismic attenuation $Q(f_s)$ along each source–receiver path (e.g. Kanamori & Given 1972), the power spectral density of the vertical displacement is

$$F_\delta(\lambda, \phi, f_s) = \int_0^{2\pi} \int_0^{\pi} \frac{S_{DF}(f_s)}{a \sin(\alpha)} P(f_s) \exp\left(\frac{-2\pi f_s a \alpha}{QU} \right) a^2 \sin(\phi')\, \mathrm{d}\lambda'\, \mathrm{d}\phi', \quad (4)$$

where a is the earth radius, α is the angular epicentral distance and $a^2 \sin\phi \mathrm{d}\lambda \mathrm{d}\phi$ is the elementary surface area. To empirically take into account the 3-D propagation or local effects on the spectrum amplitude, we introduced in eq. (4) a dimensionless parameter $P(f_s)$. This P parameter was not used in the modelling of Ardhuin *et al.* (2011). In this study, P is adjusted to fit the spectrum amplitude. The unit of F_δ is in $\mathrm{m^2\,Hz}^{-1}$ and therefore the displacement $\langle \delta^2 \rangle^{0.5}$ in metres is obtained by the square root of the integration $\sqrt{\int_{f_1}^{f_2} F_\delta \mathrm{d}f}$ in the frequency range $[f_1\, f_2]$ of interest. Because ocean wave models do not provide phase information of the pressure fluctuations, we can only compute the power spectral density of the seismic displacement, and not the displacement time series.

4 MODELLING OF NOISE SOURCES

The numerical ocean wave model is derived from the version 3.14 of the WAVEWATCH III^R code (Tolman 1991, 2008), with improved parameterizations for wind-wave generation and dissipation (Ardhuin *et al.* 2010). The model has a constant resolution of 0.5° in

latitude and longitude. At each grid point, the state is described by 31 frequencies and 24 azimuths to describe the ocean wavefield as a function of frequency and directional wave spectrum. The seismic noise sources, generated by the superposition of waves of similar frequencies and opposite directions are only stored for 15 frequencies, between 0.04 and 0.17 Hz. The model uses six hourly wind analyses from the European Centre for Medium-Range Weather Forecasts (ECMWF), daily ECMWF sea ice concentration analysis, and monthly Southern Ocean distribution statistics for small icebergs derived from Jason 1 and Jason 2 satellite altimeter data for the years 2002–2009 (Tournadre *et al.* 2008; Ardhuin *et al.* 2011). For the year 2010, the iceberg data has not been processed yet, which removes sources of noise in the Southern Ocean. An extensive description of the model and its parametrization can be found in Ardhuin *et al.* (2011). One key point of this model is that it takes into account the coastal reflections of ocean waves. The model was run without and with a spatially uniform coastal reflection. This makes it possible to obtain seismic sources that correspond to any spatially uniform coastal reflection coefficient, by a simple linear combination of the two model results. The empirical coastal reflection coefficient is non-dimensional and is set to $R^2 = 10$ per cent of the incident wave energy for continents and large islands, $R^2 = 20$ per cent for shorelines of smaller islands less that 0.5° in latitude and longitude, and $R^2 = 40$ per cent for icebergs which have nearly vertical sides. In our seismic noise computation, the reflection coefficient can vary, but the relative reflection between continent, island and iceberg is constant. Having distinguished only between these three types of shorelines is obviously very crude as the coastal reflection is known to vary from a fraction of a percent over a gently sloping beach to a maximum of about 40 per cent for a natural steep cliff. Hence the reflection coefficient should be adjusted for different coasts, as we do here.

We selected hereafter the period band 5–7 s which corresponds to the periods of the maximum average amplitude of noise spectra. Maps of the sources averaged over January and over August 2008 (Figs 3a and b) show seasonal variations of the source locations which are well correlated with the noise amplitude variations observed on Fig. 1. In the northern hemisphere, strong sources are observed between 30°N and 60°N only in January. In the southern hemisphere, the strongest sources are observed in August, but there are also sources in January, which explain why seismic noise is large for southern hemisphere stations all over the year.

Ardhuin *et al.* (2011) discussed the yearly noise sources averaged in the period band 3–12 s. Noise sources are period dependent because both the ocean wave interactions and the amplification factor (Fig. 2) depends on the period. Here we investigate the sources associated with the narrow period band 5–7 s. When averaged over one year, the strongest sources are between 30° and 60° in both hemispheres (Fig. 3c). The comparison with sources due to coastal reflection only (Fig. 3d) show that the strongest sources are in deep ocean and that sources generated by coastal reflection are dominantly along west coast of continent and islands. Similar large scale observations were made considering the period band 3–12 s (Ardhuin *et al.* 2011) but when we zoom on a particular area, source locations become different. For example, sources in the Labrador sea are stronger between the middle of the sea and the Greenland coast in the period band 5–7 s (this study) and they are stronger close the Canadian coasts when averaged over the period 3–12 s.

5 SEISMIC NOISE MODELLING

The synthetic noise power spectra are computed using eq. (4). Seismic propagation is modelled for a spherically symmetric earth (Kanamori & Given 1972). Considering our simplified two layer model, we cannot take into account varying attenuation along the paths neither focusing/defocusing effects nor reflection/refraction effects at coastlines. These effects may be important due to the large variations of crustal velocities and attenuation between oceans and

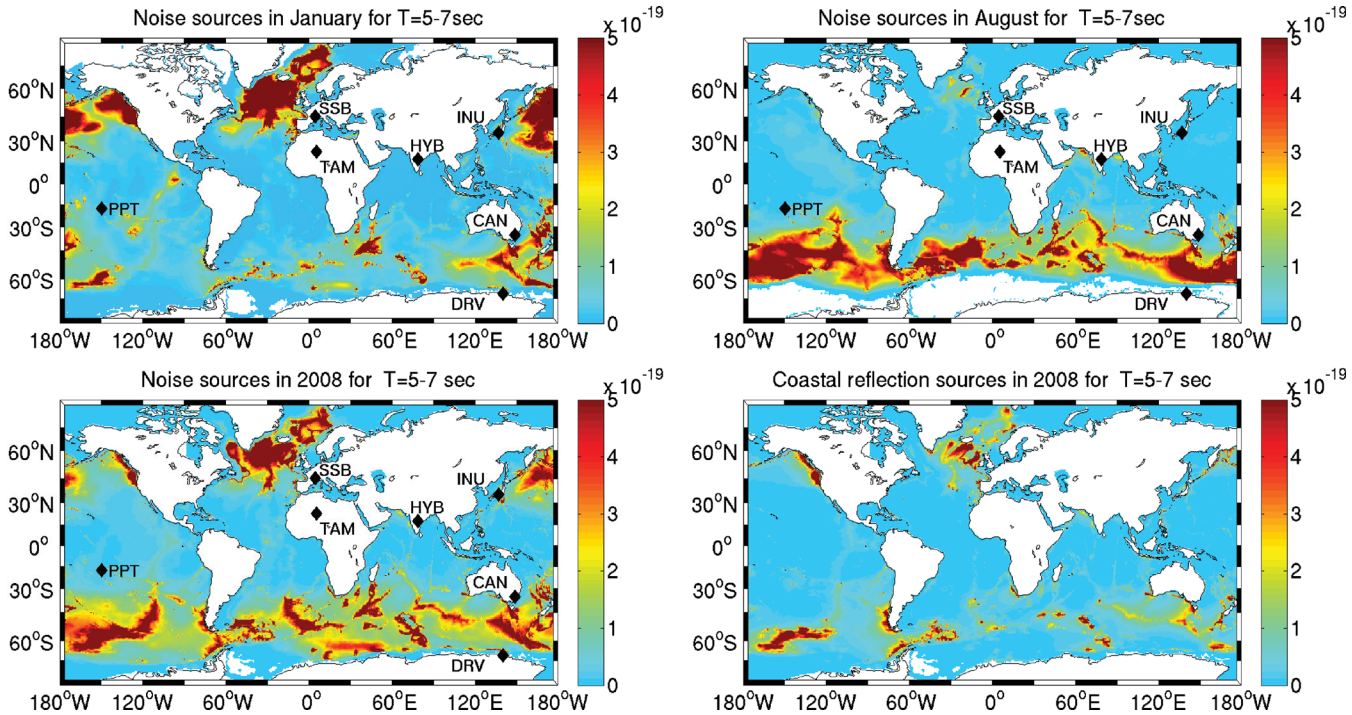

Figure 3. Noise source locations in 2008 for the period band 5–7 s in January (upper left), in August (upper right), averaged over the year (lower left), for sources generated by coastal reflection only (lower right).

continents (Nataf & Ricard 1996; Mooney *et al.* 1998). We also do not consider the thickness of sediments which may influence the amplitude of Rayleigh waves generated at a given location in the ocean (Latham & Sutton 1966; Webb 1992). But no model accurately fits surface waves in this period band even when the modelling is performed with the spectral element method to take into account 3-D propagation effects (Cupillard *et al.* 2012). To circumvent this problem, we introduced in eq. (4) a dimensionless parameter P that we vary between 0.1 and 3 to empirically take into account 3-D propagation effects on the spectra amplitude, when necessary. $P = 1$ corresponds to the case when these effects are neglected.

In eq. (4), two other parameters can be adjusted: the factor QU in the exponential and the reflection coefficient R^2. The seismic attenuation depends on the product QU and in the following, we fix the path averaged Rayleigh wave group velocity to $U = 1.8\,\mathrm{km\,s^{-1}}$ in the frequency band of interest and vary Q. The objective adjustment of the two parameters can be performed by minimizing the difference between model and observed noise. Ardhuin *et al.* (2011) showed on some examples that high correlation between data and synthetic requires different Q and reflection coefficient. Here we chose to measure the difference between data and synthetic using the correlation and the misfit to analyse the fit in phase and in amplitude and we quantify the trade-off between three parameters, Q, the reflection coefficient and the propagation parameter P. The correlation is defined as

$$r = \frac{\sum_i (d_i - \bar{d})(s_i - \bar{s})}{\sqrt{\sum_j (d_j - \bar{d})^2} \cdot \sqrt{\sum_k (s_k - \bar{s})^2}}, \tag{5}$$

where d_i and s_i are the real and synthetic spectra for the each time i. $\bar{d}$ and $\bar{s}$ are the mean of the time dependent data and synthetic spectra, respectively. The L_1 norm misfit is

$$\text{Misfit} = \frac{1}{N_d} \sum_{i=1}^{N_d} \frac{|d_i - s_i|}{|d_i|}, \tag{6}$$

where d_i and s_i are the real and synthetic spectra for the each time i and N_d the total number of time samples. For sources that occur over a broad range of distances from the recording stations, increasing Q augments the relative contribution from distant sources and modify both the correlation and the misfit as it increases the synthetic noise level. For sources always located at the same distance, a change in Q has no effect on the correlation and only affects the misfit. Increasing the reflection coefficient factor R^2 increases the contribution of sources located near the coast and affects both correlation and misfit. Varying the parameter P enables to adjust the spectra amplitude which modify the misfit but it has no effect on the correlation. When it is neglected, one may obtain at some stations unrealistic attenuation and coastal reflection values which would modify the pattern of the sources that contribute to the noise recorded by a given station.

5.1 Modelling noise in various environments over one year

To show how these parameters affect the spectra, we first computed synthetic spectra using the ocean wave hindcasts without and with 10 per cent of coastal reflection for the year 2008. We consider fixed P parameter and varying Q. The period range of interest is narrow, between 5 and 10 s and we keep Q constant over the period band. Fig. 4 shows real and synthetic noise spectra (in dB with respect to acceleration) for stations in various environments. Seismic spectra are averaged over the year 2008 and plotted for two continental stations SSB in France and CAN in Australia and one island station PPT in French Polynesia. The real spectral amplitudes are between −130 and −120 dB for both continental stations SSB and CAN and higher between −105 and −120 for the island station PPT. These amplitudes are well recovered by the synthetic spectra. We used $P = 1$ for SSB and CAN and $P = 1.9$ for PPT. The selection of these P values is discussed later in this section. The spectrum shapes in acceleration are characterized by a gentle slope for periods shorter than about 7 s and a steep slope for periods between 7 and 14 s. Fig. 4 shows that for the island station PPT, the spectrum shape and amplitude can be correctly reproduced without coastal reflection, considering $Q = 450$ and that the modelling with strong coastal reflection over predict the amplitude of long period (above 8 s) spectrum. We can infer that there is little effect of coastal reflection in the vicinity of the station. For the continental station SSB in France, the spectrum shape is better reproduced in the period band 3–7 s by the synthetic spectrum without coastal reflection but the amplitude at longer period is better reproduced with coastal reflection. For the last station CAN in Australia, only the modelling with coastal reflection enables to reproduce the spectrum shape in the entire period band. The importance of coastal reflection is confirmed by Fig. 3(d) which shows that strong sources due to coastal reflection are present close to the two stations CAN and SSB. This comparison of the real and synthetic spectra further shows that sources generated by coastal reflection are particularly important for the long period data (9–12 s). This is not surprising because the rarity of long period storms makes coastal reflection the best mechanism for generating long period microseisms. Noise sources generated by ocean wave coastal reflection are dominantly observed along the western coast due to the direction of the incident waves mostly travelling from west toward east.

To investigate the trade-off between parameters, we considered the temporal variations of the spectra in the period band 5–7 s. Spectra are computed every 6 hr over the year 2008 and used to compute the correlation (Fig. 5, left-hand side) and misfit (Fig. 5, right-hand side) with the synthetic spectra for varying parameters. For the station CAN in Australia, we see that the highest correlation and lowest misfit are achieved for consistent values of the attenuation Q, between 130 and 180 and reflection coefficient R^2 between 4 and 10 per cent. These results are obtained for $P = 1$. On Fig. 6, we further show in red as a function of P, the minimum misfit (left-hand side), the corresponding attenuation (middle) and reflection coefficient (right-hand side). We also plotted with circles all misfits within 5 per cent of the minimum value and the corresponding Q and R^2. We observe a continuous increase of the misfit as a function of P and that the smallest value of P corresponds to unrealistic high and strongly varying values for Q and R^2. Clearly, P cannot be resolved considering the misfit. We arbitrarily choose $P = 1$. We also plotted in grey on Fig. 6 the range of R^2 and Q that provide the highest correlation. Correlation does not depend on the relative amplitudes of the signals and therefore is independent of P. We see that Q and R^2 values estimated from the correlation are consistent with those estimated from the misfit (circles) when $P = 1$. It would not be the case for small values of P.

For station SSB in France, the shape of the minimum misfit curve as a function of P is similar to that of CAN and we also select $P = 1$ (Fig. 6). Considering $P = 1$, Fig. 5 shows that the highest correlation is achieved for $Q > 200$ and $R^2 > 1.5$ per cent but the correlation does not constrain the maximum values for Q and R^2. Considering the lowest misfit values, we further select Q between 230 and 280 and R^2 between 1 and 5 per cent which is in the range of acceptable values considering the correlation. For comparison, Ardhuin *et al.*

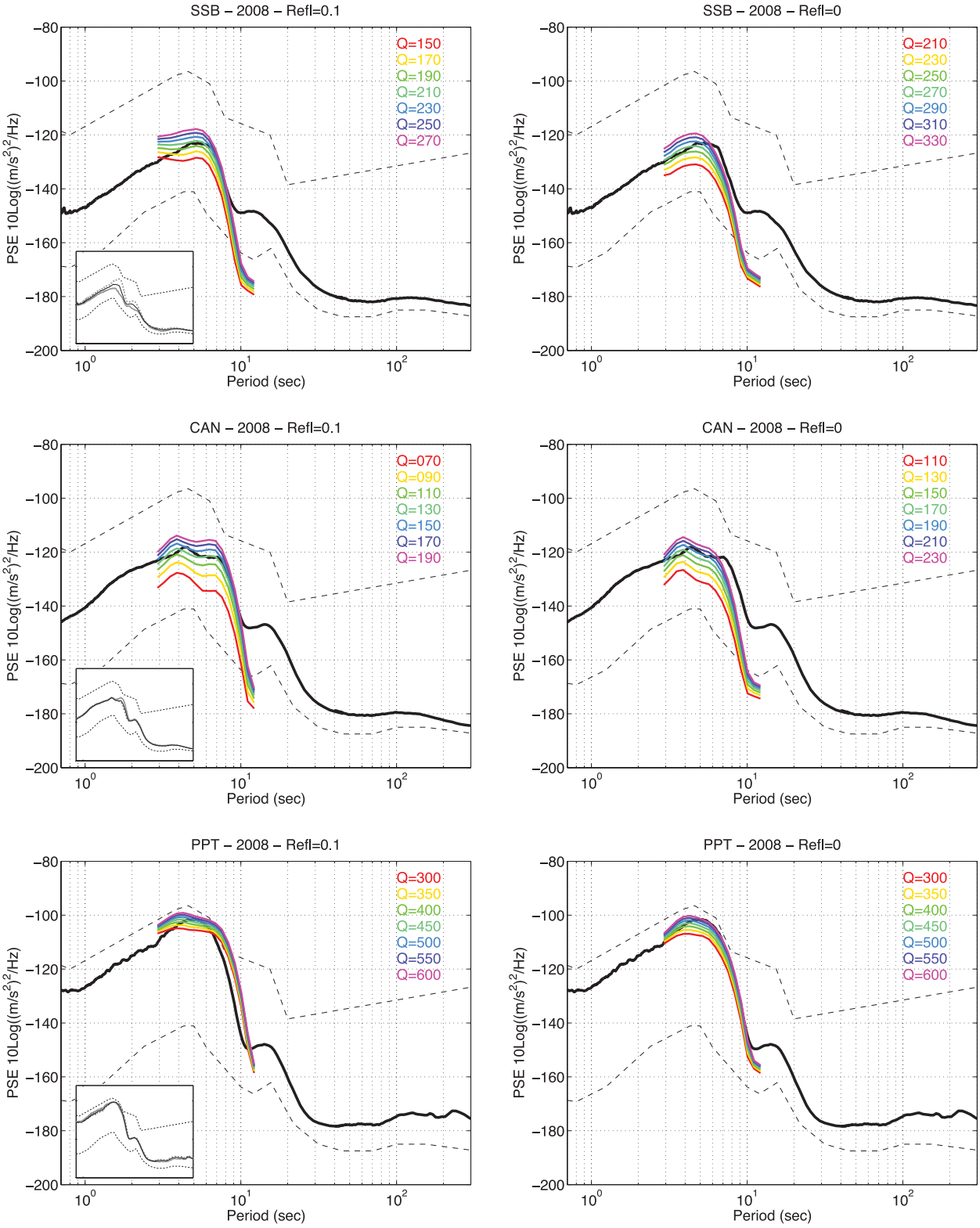

Figure 4. Real (black) and synthetic (colour) power spectra averaged over the year 2008 for two continental stations, SSB in France and CAN in Australia and an island station PPT in french Polynesia (Tahiti). Synthetic spectra are computed with the IOWAGA ocean wave model with (left-hand side, $R^2 = 0.1$) and without (right-hand side, $R^2 = 0$) ocean wave coastal reflection. Synthetic spectra are computed for different fixed attenuation Q whose value is written in colour on each plot. Inlets show averaged power spectra for 1 year (solid black line), January (dashed grey line) and August (solid grey line).

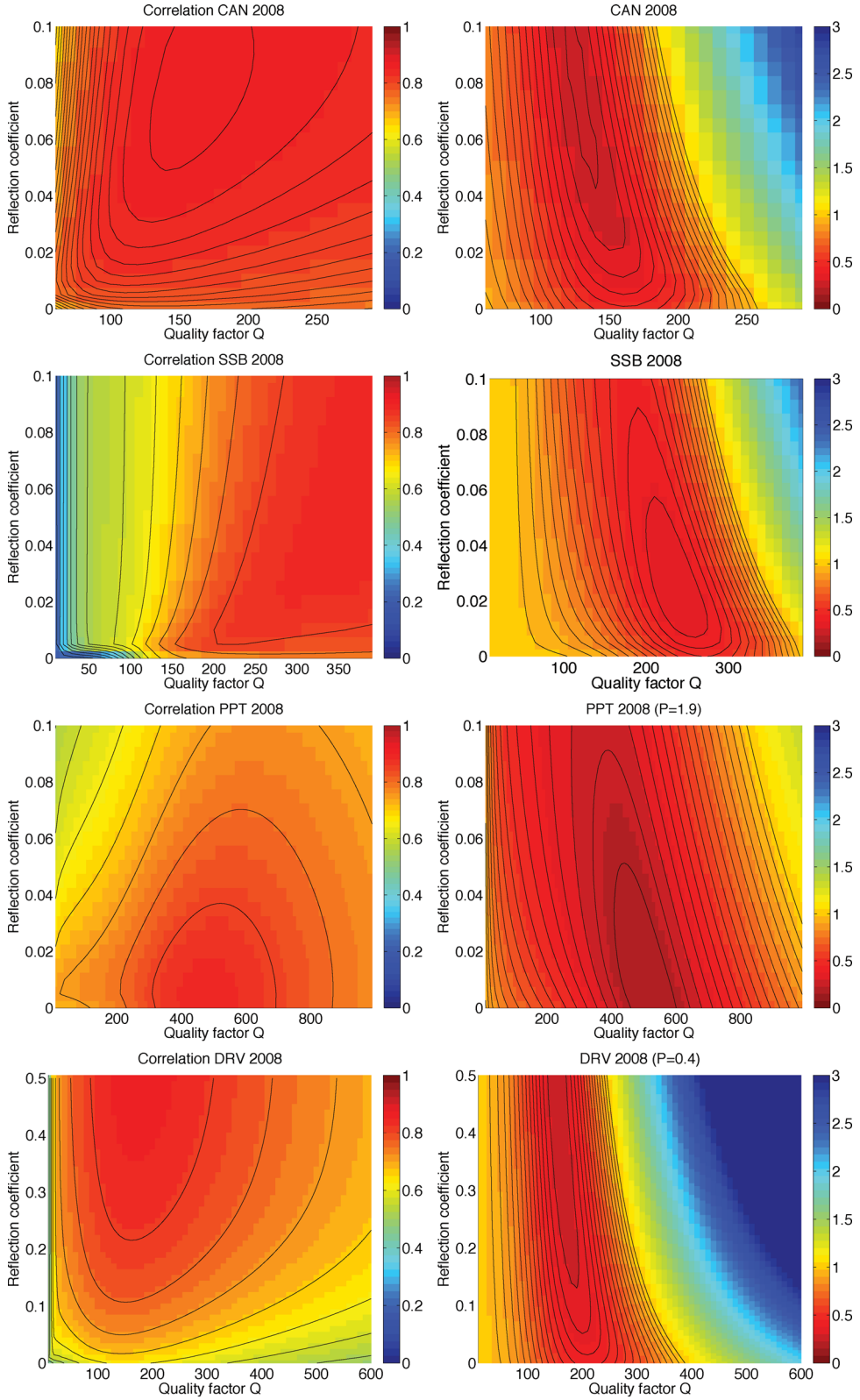

Figure 5. Correlation (left-hand side) and misfit ($L_1 norm$, right) between real and synthetic spectra as a function of seismic attenuation and ocean wave coastal reflection coefficient for for two continental stations, CAN in Australia and SSB in France and an island station PPT in french Polinesia (Tahiti).

(2011) used $Q = 260$ and $R^2 = 5$ per cent (at $T = 5$ s) in their modelling of the same station which is in the range of acceptable value as shown on Fig. 6. They do not use P in their modelling and we have shown that for that station the misfit and correlation provide similar parameters using $P = 1$ which means that local or 3-D propagation effects can be neglected.

Considering the island station PPT in Tahiti, the curve of the minimum misfit as a function of P is minimum for $P = 1.9$ (Fig. 6).

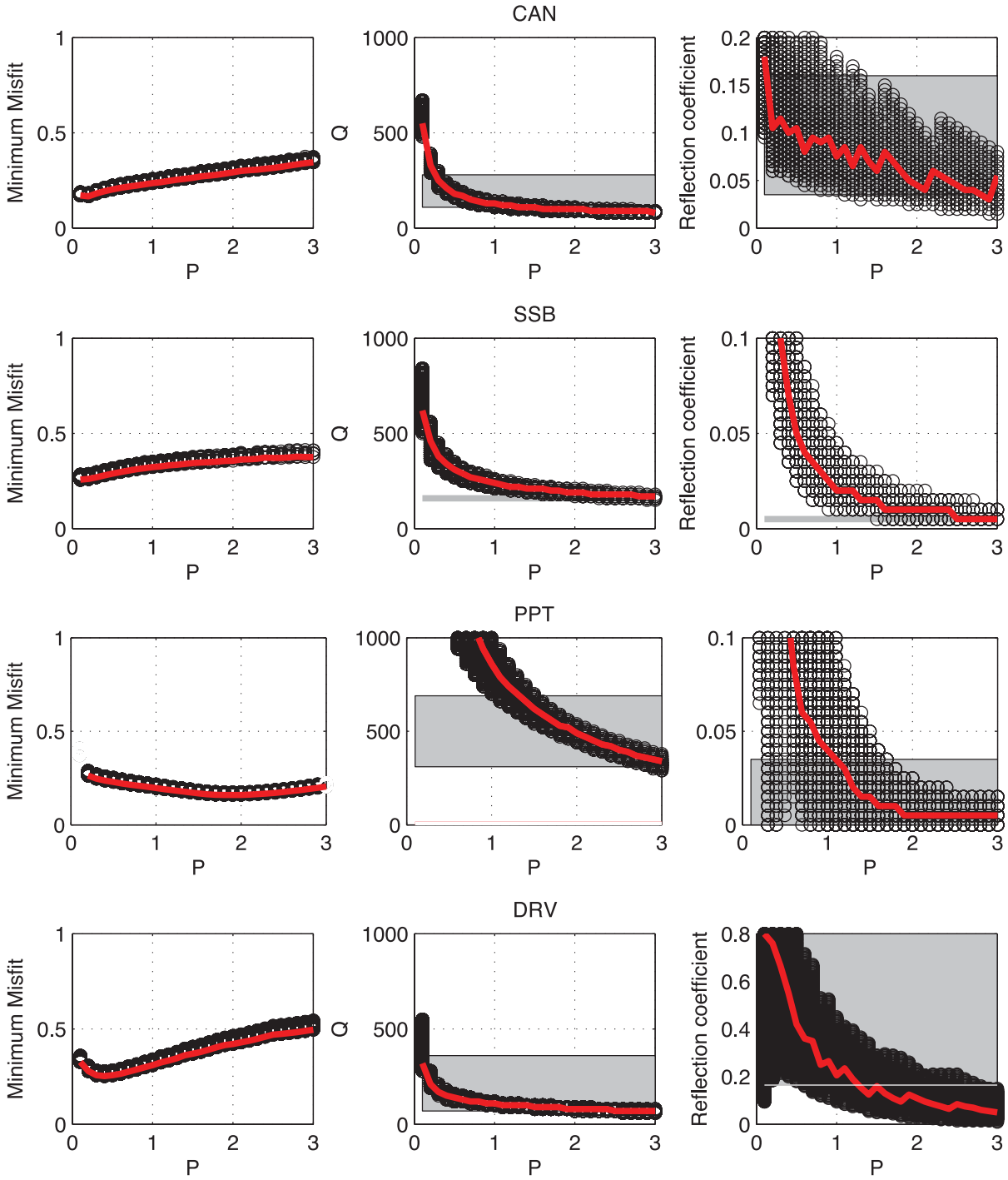

Figure 6. In red is plotted the lowest misfit as a function of the propagation parameter P (left-hand side) and the corresponding attenuation (middle) and reflection coefficient (right-hand side). Circles correspond to all misfit values within 5 per cent of the minimum value (left-hand side) and the corresponding Q (middle) and R^2 (right-hand side). The grey area corresponds the highest correlation values (left-hand side) and the corresponding values for Q (middle) and R^2 (right-hand side). For station SSB, only the lower limit is given for the attenuation (grey line in the top middle figure) as there is no constraint on the highest limit from the correlation.

For $P = 1$ or smaller, we obtain unrealistic and strongly varying values for Q (up to 10.000) and R^2. We use $P = 1.9$ and Figs 5 and 6 show that the smallest misfit is achieved for Q between 400 and 600 and R^2 between 0 and 5 per cent. Similar values values for Q and smaller R^2 range between 0 and 3 per cent are obtained when considering the correlation. For that station, coastal reflection can be neglected in the modelling. Ardhuin *et al.* (2011) modelled another island station in Hawai (KIP) and used $Q = 700$ and $R^2 = 5$ per cent in their modelling. In agreement with this study of PPT station, they observe at KIP station that R^2 has little influence on the modelling but their Q is probably overestimated because as they do not use P and the large amplitude is fitted by increasing Q. For the south Pacific island station PPT, other effects such as local or 3-D propagation effects must be taken into account.

Finally, for station DRV in Antarctica, the curve of the minimum misfit as a function of P is minimum for $P = 0.4$ (Fig. 6). Considering $P = 0.4$, the lowest misfit and highest correlation consistently correspond to Q between 150 and 250 and R^2 higher than 15 per cent. Fig. 5 further shows that the upper limit for the reflection coefficient cannot be resolved.

After selecting the range of acceptable values for Q, R^2 and P, we modelled the spectra temporal variations with and without coastal reflection and compare them with the real spectra. We use $P = 1$ for SSB and CAN, $P = 1.9$ for PPT and $P = 0.4$ for DRV. In Fig. 7, spectra are computed considering (Q, R^2) that correspond to the smallest misfit. These (Q, R^2) values are in the range defined earlier. We obtain a remarkable agreement between real and synthetic spectra for all stations (black and green curves on Fig. 7).

For the station CAN in Australia, synthetic spectrum computed with $Q = 130$ and high coastal reflection coefficient provides a much better fit to the real spectra than that without coastal reflection(red curve in Fig. 7). The correlation between data and synthetic is 0.86 when 6 per cent of coastal reflection is taken into account and 0.76 for modelling without coastal reflection. In Australia strong sources are generated by wave reflections at the western and southern coasts (Fig. 3d). We observed no significant variations of the noise amplitude spectra in the period band 5–7 s between winter and summer (Fig. 7) which is due to the existence of strong sources all over the year in the oceans surrounding Australia as shown on Fig. 2.

For station SSB, a quality factor of $Q = 240$ corresponds to the e-folding distance of 825 km for displacement at a period of 6 s which means that station SSB records sources in the North Atlantic Ocean and Mediterranean Sea. As seen on Fig. 2, sources located in the northern part of North Atlantic ocean, south of Greenland, are strongly amplified and they dominate the seismic noise recorded by this station, particularly in winter (Fig. 3). This explains the higher noise amplitude during winter that is well reproduced by synthetic spectra (Fig. 7). Neglecting the coastal reflection decreases the correlation between data and synthetic from 0.87 (for $R^2 = 2$ per cent) to 0.78 (green and red synthetic spectra respectively on Fig. 7).

For the island station PPT, in the South Pacific Ocean, we show the modelling for $R^2 = 4$ per cent, $Q = 450$ and $P = 1.9$. The correlation between real and synthetic spectra is $r = 0.88$ with and without coast reflection which confirms the small influence of coastal reflection for that station. It can be explained by the location of the station in a small island in the middle of the ocean that is far away from long coasts. The e-folding distance corresponding to $Q = 450$ is 1547 km for displacement and a period of 6 s which means that the station records seismic signal generated by sources in a large portion of the Pacific Ocean. For that station, the use of $P = 1.9$, means that our simplified model alone underpredicts the magnitude of the amplitude variations but the temporal variation of the noise is correctly recovered.

For our last station, DRV in Antarctica, we show the modelling for $P = 0.4$, $Q = 100$ and $R^2 = 0.15$ (Fig. 7). Synthetic spectra reproduce the decrease of noise between February and December during local winter when sea ice is formed around the station and that open sea in winter is located several hundred of kilometres away from the station. We further see that for this station, coastal reflection effect is more important in summer than in winter, that is, when noise sources can be closer from the station due to the absence of ice. However, this may be a bias of our model that does not include reflection by ice floes in the marginal ice zone. For that station, our model would over predict the spectral magnitude without introducing $P = 0.4$.

For each station, the comparison between synthetic spectra computed for ocean models with and without coastal reflection (Fig. 7) shows that the largest noise peaks are mostly generated by sources in deep ocean and that coastal reflection generates numerous sources of smaller amplitude that provide the background amplitude of seismic spectra. This is observed for all the stations in this study, each of the spectra being modelled with a reflection coefficient appropriate to the station/area. The reflection coefficients are ranging between 2 and 15 per cent for the different stations. We obtained Q ranging between 100 and 600 for these stations. These values are determined empirically but are consistent with the range of theoretical values computed for continental or oceanic model considering CRUST2.0 or 3SMAC models (Nataf & Ricard 1996; Mooney *et al.* 1998).

5.2 Modelling long-term noise variations

To determine the validity of the empirical parameters determined over the year 2008 for the long-term modelling of noise, we repeated our analysis of the trade-off between P, Q and R^2 between 2003 and 2010. For each station and each year, we computed spectra for a wide range of P, Q, R^2 and selected the optimum P values from the misfit analysis similar to Fig. 6. For each station, we retrieved the same P as for 2008. We then used these P values and recomputed the misfit and correlation as a function of Q and R^2. On Fig. 8, we show for each year, the minimum misfit (left-hand side) and the corresponding Q (middle) and R^2 (right-hand side). We plotted with circle all misfit values within 5 per cent of the minimum misfit and the corresponding Q and R^2. We also plotted the highest correlation values and corresponding Q and R^2 (in grey). We clearly see that the minimum misfit and highest correlation values are stable over the 8 yr. There is a good agreement between Q and R^2 values associated with the lowest misfit and with the highest correlation for every year and these values are stable other the years. The stability of the all three fitted parameters demonstrate the robustness of our approach.

Fig. 9 shows the daily noise power spectra for the year 2003–2010 in the period band 3–10 s. We observe an excellent agreement between real and synthetic spectra. The modelling also correctly reproduce the seasonal variations with maximum noise between November and February for stations in France (SSB), Japan (INU) and Algeria (TAM) in the northern hemisphere and between June and September for the station in Australia (CAN) in the southern hemisphere. We even reproduce the peculiar spectra of the Antarctica station (DRV) with a maximum of noise during local summer. We model low amplitude at the Algerian station (TAM) in the middle of the African continent, and the intermediate amplitude of the most other stations. For all these stations, our analysis of the trade-off between parameters did not enable to resolve P and we used $P = 1$. Only for the island station (PPT) and the polar station DRV we used respectively $P = 1.9$ and $P = 0.4$. For these two stations either 3-D propagation effects and local site effects should be taken into account or the wave model amplitude is not accurate or both.

Fig. 10 presents a zoom on the daily spectra over the year 2008 for the stations SSB and DRV. This figure shows that for the continental station SSB in France, the dates, the frequency content and relative amplitude of each noise peak are well reproduced all over the year. The strongest microseismic signals are in the period band 4–8 s. Some large storms in winter generate seismic noise at longer period

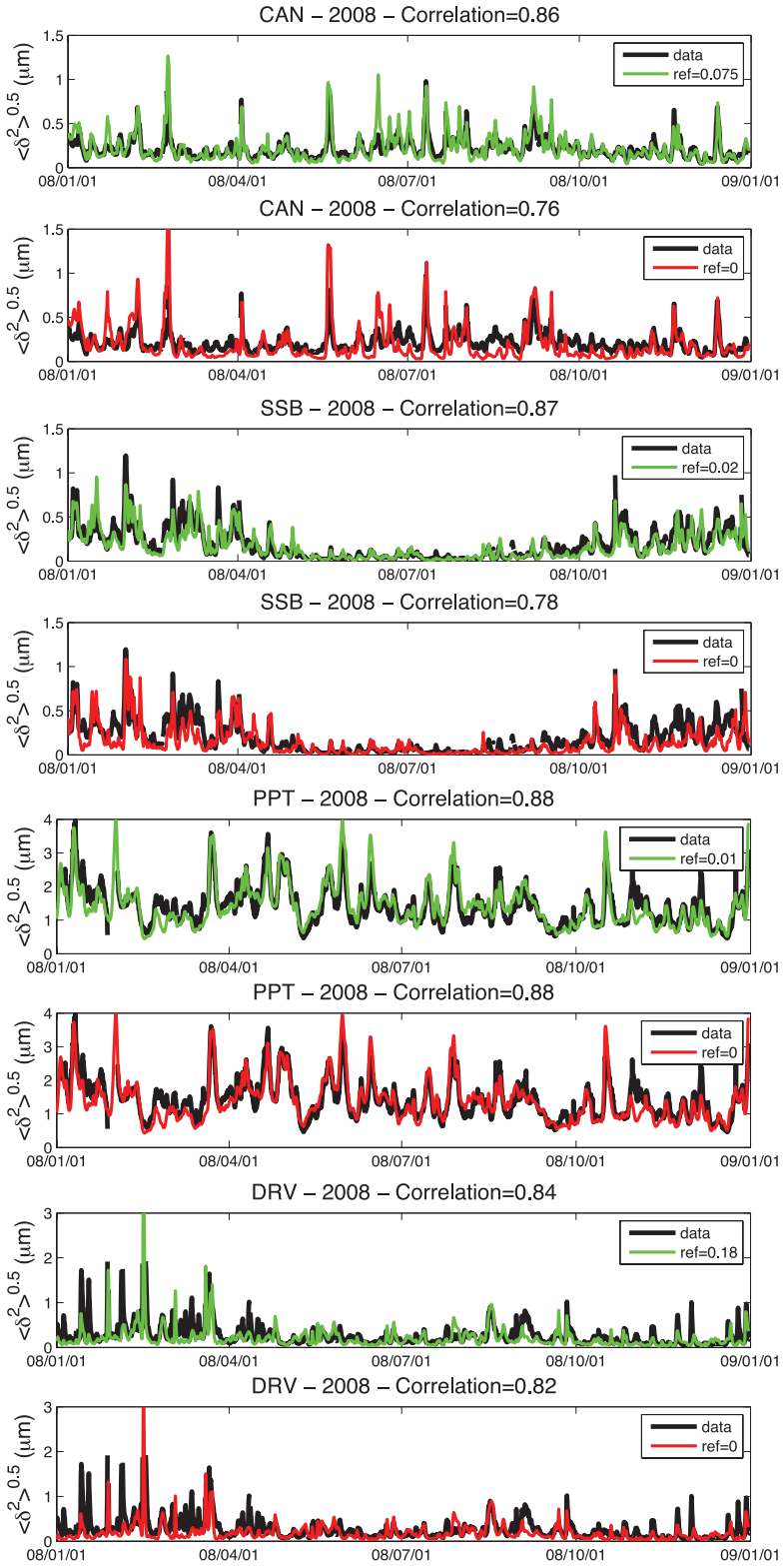

Figure 7. Real (black) and synthetic (colour) power spectra variations over year in displacement (m) for two continental stations, CAN in Australia and SSB in France, an island station PPT in french Polynesia (Tahiti) and a station in Antarctica DRV. Synthetic spectra are computed with (green) and without (red) taking into account ocean wave coastal reflection.

up to 10 s or more. In summer, the maximum period of the peaks is smaller, around 8 s. Such figure can be used to select seismic signals corresponding to quiet days in a given period band. It can also be used to identify the strongest sources recorded by a station in a given period band which can then be located using the ocean wave maps such as presented in Fig. 11 for 2008 October 9.

At the station DRV, in Antarctica, the high noise level between December and April is well reproduced by the synthetic spectra

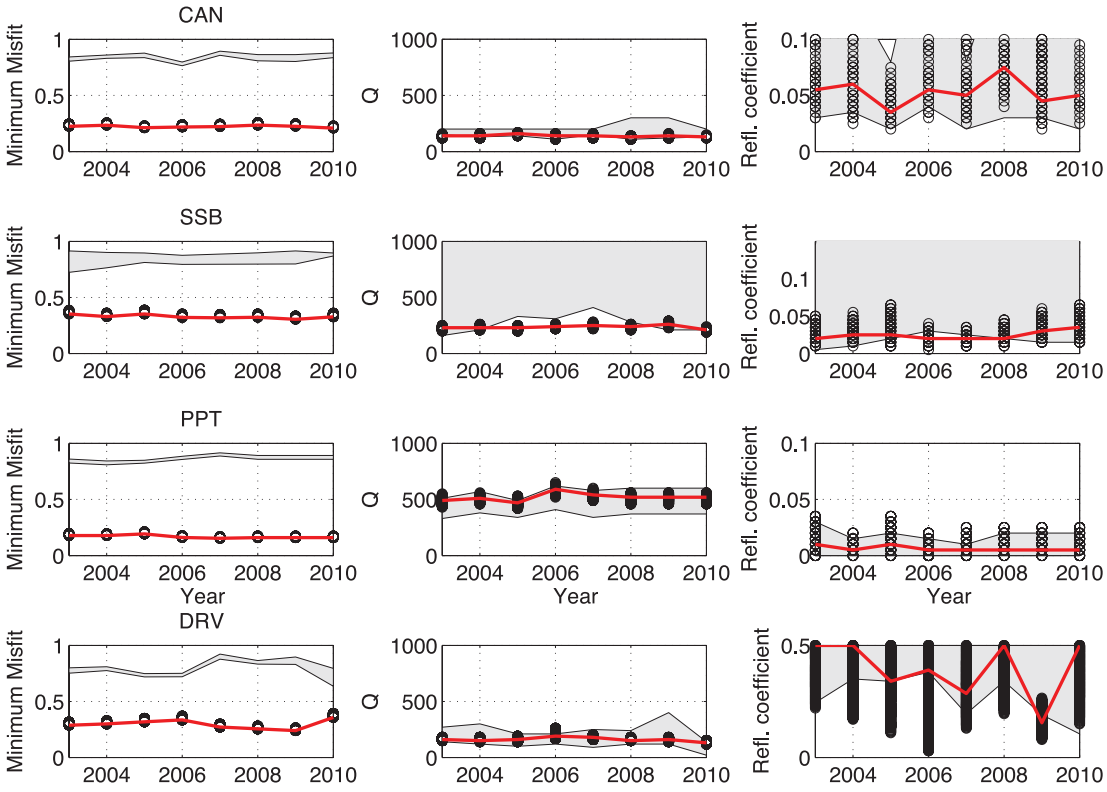

Figure 8. For years 2003 to 2010, the lowest mistfit (left-hand side) and the corresponding attenuation (middle) and reflection coefficient (right-hand side) are plotted in red. Circles correspond to all the misfit values within 5 per cent of the minimum value (left-hand side) and the corresponding Q (middle) and R^2 (right-hand side). The grey areas correspond to the highest correlation values (left-hand side) and the corresponding values for Q (middle) and R^2 (right-hand side).

(Fig. 10). Then, starting in April, there is an abrupt drop of the noise amplitude between 3 and 6–7 s, whereas at longer period we observe high noise amplitude up to longer periods than at the beginning of the year. The modelling correctly reproduces the decrease of noise between May and November, but it overestimates the relative noise level in the period band 3–6 s and underestimates longer period noise (6–10 s). A possible explanation is that in the model all waves are suppressed when the sea ice fraction exceeds 0.7, whereas in reality the longer waves may be able to propagate through long distances of ice-covered ocean, and thus reach the coast close to DRV (Liu & Mollo-Christensen 1988). Also, the model does not include reflections by ice floes in the marginal ice zone, which are known to be strong scatterers of waves, and thus a potential large source of seismic noise (Meylan *et al.* 1997). Nevertheless, even in winter, the dates of the noise peaks are well reproduced.

6 CONCLUSION

We selected seven stations representative of the various environments on earth, that is continent, island and polar area in both hemispheres which show seasonal seismic noise variations that are stable over more than 20 yr. We then model this noise using the theory of Longuet-Higgins (1950) generalized by Hasselmann (1963) for random ocean gravity waves and using an ocean wave model that takes into account ocean wave coastal reflection. The strongest sources are located in deep ocean and sources generated by coastal reflection are dominantly along the west coasts. We further show that the strongest sources are located at high latitude between 30° and 60° in both hemisphere during local winter and that strong sources are present around Antarctica all over the year. The amplitude and exact location of the sources vary with the frequency.

We quantify the trade-off in the modelling between ocean wave coastal reflection, seismic attenuation and a parameter, P, representing the 3-D seismic propagation or local effects. They all affect the seismic spectrum amplitude and we discuss their adjustments. Whereas for most stations, one simplified modelling reproduce the absolute amplitude of the noise spectra without the extra parameter P ($P = 1$), for the island station PPT and the polar station DRV the absolute amplitude is respectively underestimated ($P = 1.9$) and over estimated ($P = 0.4$) and 3-D propagation or local effects should be more accurately modelled. Alternatively, the wave model may not be accurate in the vicinity of these stations.

The modelling parameters are different for the the various stations but the analysis of many years shows the stability of the fitted parameters which demonstrates the robustness of our approach. We observe a good agreement between real and synthetic spectra. We correctly reproduce the dates and frequency content and relative amplitude of each individual noise peak. The strongest peaks observed in noise spectra are generated by deep ocean sources whereas coastal reflections generate numerous smaller sources that contribute to the background noise level. The best fit of seismic spectra is achieved when both deep ocean and coastal reflection sources are taken into account. Coastal reflection effect is negligible only for the Pacific island station PPT. The modelling also reproduces the peculiar noise spectrum variation in Antarctica station DRV which is related to the presence of sea ice around the stations.

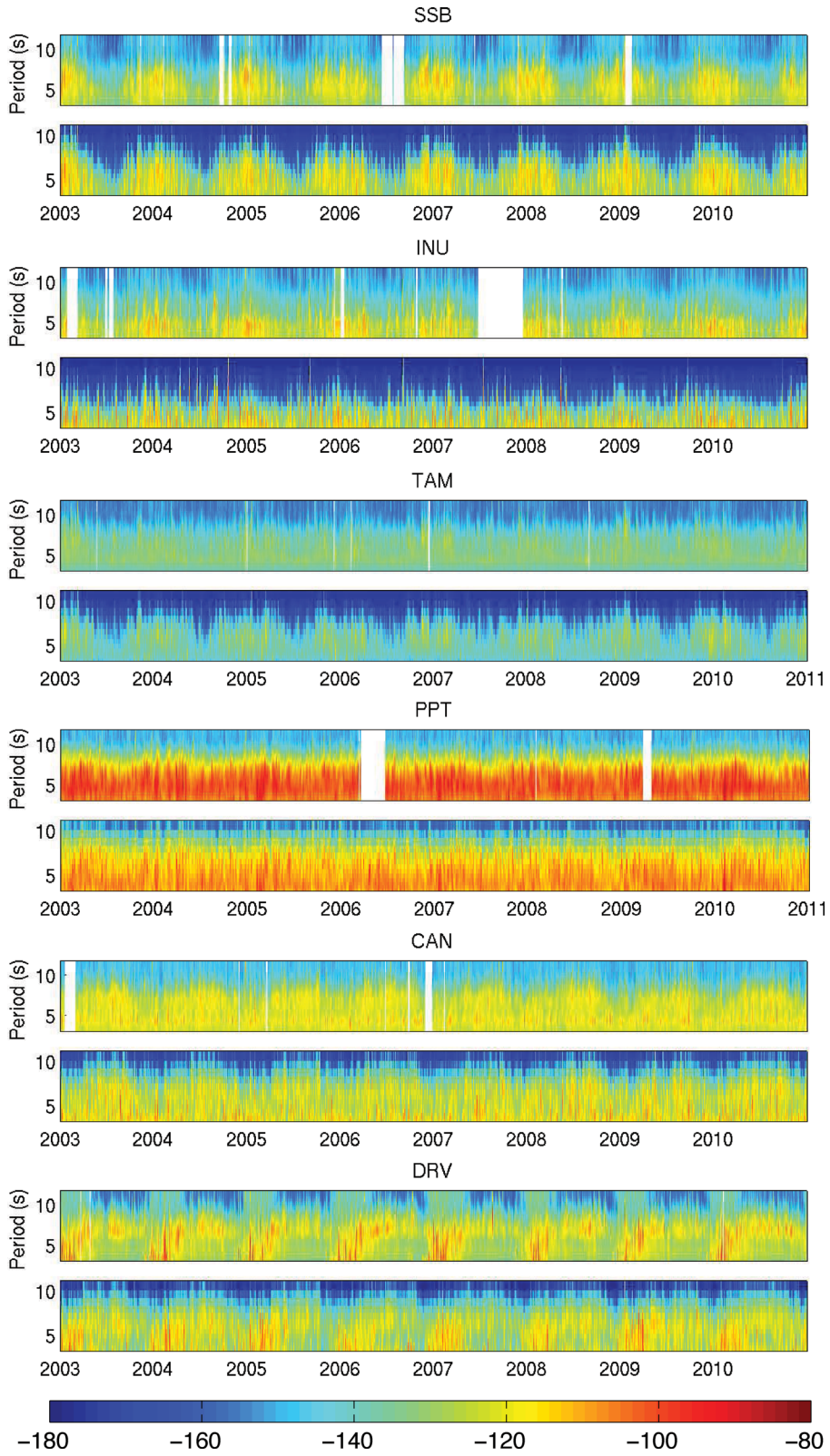

Figure 9. Real and synthetic noise power spectra variations for stations in France (SSB), Japan (INU), Algeria (TAM), French Polynesia (PPT), Australia (CAN) and Antarctica (DRV). For each station, real (top panel) and synthetic (bottom panel) daily spectra are plotted in dB with respect to acceleration (colour) for the years 2003–2010 and the period band 3–10 s.

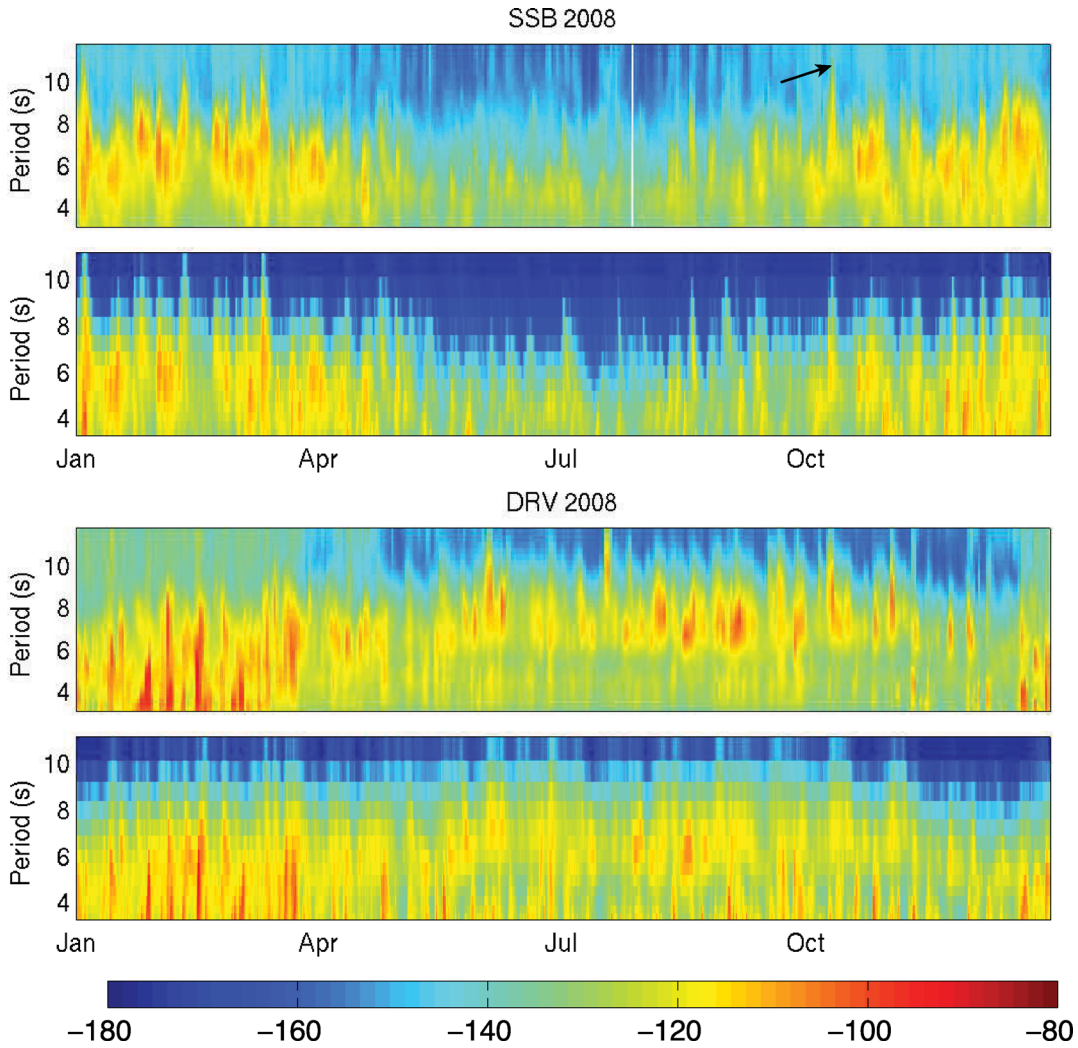

Figure 10. Real and synthetic noise power spectra variations for stations in France (SSB) and in a small island close to Antarctica (DRV). For each station, real (top panel) and synthetic (bottom panel) daily spectra are plotted in dB with respect to acceleration (colour) for the years 2008 and the period band 3–10 s The noise peak designed by the arrow corresponds to the source shown on Fig. 11.

Modelling seismic noise is a useful new tool for selecting particular noise data such as, for example, the strongest peaks and further investigating the corresponding sources. Narrow noise sources may also be used for new tomography studies. Parameters associated with the different environments that were determined in this study can be used for future noise studies.

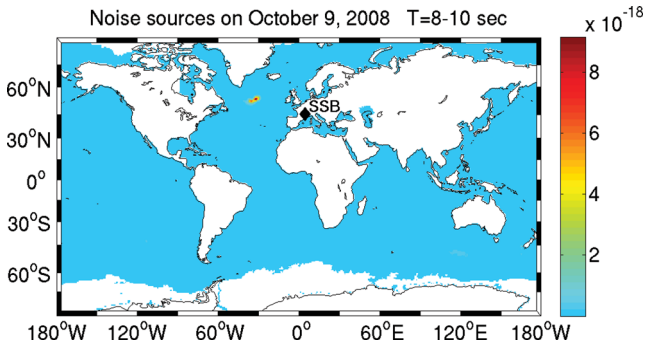

Figure 11. Noise source location on 2008 October 9 for the period band 8–10 s.

ACKNOWLEDGMENTS

This is IPGP contribution number 3325. The authors thank's GEOSCOPE network for providing the data used in this study. MS acknowledges support by ILink2010-0112 and CGL2009-09727 (Rifsis).

REFERENCES

Ardhuin, F. *et al.*, 2010. Semi-empirical dissipation source functions for wind-wave models: part i, definition, calibration and validation, *J. Phys. Oceanogr.,* **40**(9), 1917–1941.

Ardhuin, F., Stutzmann, E., Schimmel, M. & Mangeney, A., 2011. Revealing ocean wave sources of seismic noise, *J. geophys. Res.,* **116,** C09004, doi:10.1029/2011JC006952.

Ardhuin, F., Balanche, A., Stutzmann, E. & Obrebski, M., 2012. From seismic noise to ocean wave parameters: methods, *J. geophys. Res.,* **117,** C05002, doi:10.1029/2011JC007449.

Aster, R., McNamara, D. & Bromirski, P., 2008. Multi-decadal climate-induced variability in microseisms, *Seism. Res. Lett.,* **79,** doi:10.1785/gssrl.79.2.194.

Bernard, P., 1990. Historical sketch of microseisms from past to future, *Phys. Earth planet. Inter.,* **63,** 145–150.

Brenguier, F., Shapiro, N., Campillo, M., Ferrazini, V., Duputel, Z., Coutant, O. & Nercessian, A., 2008a. Towards forecasting volcanic eruptions using seismic noise, *Nat. Geosci.,* **1,** 126–130, doi:10.1038/ngeo104.

Brenguier, F., Campillo, M., Hadziioannou, C., Shapiro, N.M., Nadeau, R.M. & Larose, E., 2008b. Postseismic relaxation along the San Andreas Fault at Parkfield from continuous seismological observations, *Science,* **321,** 1478–1481.

Bromirski, P. & Duennebier, F., 2002. The near-coastal microseism spectrum: spatial and temporal wave climate relationships, *J. geophys. Res.,* **107,** B82166, doi:10.1029/2001JB000265.

Bromirski, P., Flick, R.E. & Graham, N., 1999. Ocean wave height determined from inland seismometer data: implications for investigating wave climate changes in the ne pacific, *J. geophys. Res.,* **104**(C9), 20753–20766.

Cessaro, R.K., 1994. Sources of primary and secondary microseisms, *Bull. seism. Soc. Am.,* **84**(1), 142–148.

Chevrot, S., Sylvander, M., Ponsolles, C., Benahmed, S., Lefevre, J.M. & Paradis, D., 2007. Source locations of secondary microseisms in western europe: evidence for both coastal and pelagic sources, *J. geophys. Res.,* **112,** B11301, doi:10.1029/2007JB005059.

Cupillard, P., Delavaud, E., Burgos, G., Festa, G., Vilotte, J.-P., Capdeville, Y. & Montagner, J.-P., 2012. RegSEM: a versatile code based on the Spectral Element Method to compute seismic wave propagation at the regional scale, *Geophys. J. Int.,* **188**(3), 1203–1220, doi:10.1111/j.1365-246X.2011.05311.x.

Friedrich, A., Kruger, F. & Klinge, K., 1998. Ocean-generated microseismic noise located with the grafenberg array, *J. Seismol.,* **2,** 47–64.

Gerstoft, P. & Tanimoto, T., 2007. A year of microseisms in southern california, *Geophys. Res. Lett.,* **34,** L20304, doi:10.1029/2007GL031091.

Grevemeyer, I., Herber, R. & Essen, H., 2000. Microseismological evidence for a changing wave climate in the northeast atlantic ocean, *Nature,* **408,** 349–352.

Grob, M., Maggi, A. & Stutzmann, E., 2011. Observations of the seasonality of the antarctic microseismic signal and its association to sea ice variability, *Geophys. Res. Lett.,* **38,** L11302, doi:10.1029/2011GL047525.

Hasselmann, K., 1963. A statistical analysis of the generation of microseisms, *Rev. Geophys.,* **1,** 177–209.

Haubrich, R. & McCamy, K., 1969. Microseisms: coastal and pelagic sources, *Rev. Geophys.,* **7,** 539–571.

Kanamori, H. & Given, J., 1972. Use of long period surfeace waves for rapid determination of earthquake-source parameters, *Phys. Earth planet. Inter.,* **27,** 8–31.

Kedar, H., Longuet-Higgins, M., Webb, F., Graham, C., Clayton, R. & Jones, C., 2008. The origin of deep ocean microseisms in the north atlantic ocean, *Proc. R. Soc. A.,* **464**(2091), 777–793, doi:10.1098/rspa.2007.0277.

Koper, K. & Foy, B., 2008. Seasonal anisotropy in short-period seismic noise recorded in south asia, *Bull. seism. Soc. Am.,* **96,** 3033–3045, doi: 10.1785/0120080082.

Latham, G. & Sutton, G., 1966. Seismic measurements on the ocean floor, *J. geophys. Res.,* **71,** 2545–2573.

Liu, A.K. & Mollo-Christensen, E., 1988. Wave propagation in a solid ice pack, *J. Phys. Oceanogr.,* **18,** 1702–1712.

Longuet-Higgins, M., 1950. A theory of the origin of microseisms, *Phil. Trans. Roy. Soc.,* **243,** 1–35.

Meylan, M., Squire, V. & Fox, C., 1997. Towards realism in modeling ocean wave behavior in marginal ice zones, *J. geophys. Res.,* **102**(C10), 22 981–22 991.

Miche, A., 1944. Mouvements ondulatoires de la mer en profondeur croissante ou décroissante. Première partie. Mouvements ondulatoires périodiques et cylindriques en profondeur constante, *Annales des Ponts et Chaussées,* **114,** 42–78.

Montagner, J.-P. *et al.*, 1994. The French pilot experiment ofm/sismobs: first scientific results on noise level and event detection, *Phys. Earth planet. Inter.,* **84,** 321–336.

Mooney, W., Laske, G. & Masters, G., 1998. Crust 5.1: A global crustal model at 5deg x 5deg, *J. geophys. Res.,* **103,** 727–747.

Nataf, H. & Ricard, Y., 1996. 3 smac an a priori tomographic model of the upper mantle based on geophysical modeling, *Phys. Earth planet. Inter.,* **95,** 101–122.

Nishida, K., Kawakatsu, I., Fukao, Y. & Obara, K., 2008. Background love and rayleigh waves simultaneously generated at the pacific ocean floors, *Geophys. Res. Lett.,* **35,** L16307, doi:10.1029/2008GL034753.

Nishida, K., Montagner, J. & Kawakatsu, I., 2009. Global surface wave tomography using seismic hum, *Science,* **326**(5949), 112, doi:10.1126/science1176389.

Peterson, J., 1993. Observations and modeling of seismic background noise, USGS Open-File Report, 93-322, 95 pp.

Rhie, J. & Romanowicz, B., 2006. A study of the relation between ocean storms and the earth's hum, *Geochem. Geophys. Geosyst.,* **7**(10), doi:10.1029/2006GC001274.

Schimmel, M., Stutzmann, E. & Gallart, J., 2010. Using instantaneous phase coherence for signal extraction from ambient noise data at a local to a global scale, *Geophys. J. Int.,* **184,** 494–506, doi:10.1111/j.1365-246X.2010.04861.x.

Schimmel, M., Stutzmann, E., Ardhuin, F. & Gallart, J., 2011. Earth's ambient microseismic noise, *Geochem. Geophys. Geosyst.,* **12,** Q07014, doi:10.1029/2011GC003661.

Schulte-Pelkum, V., Earle, P. & Vernon, F., 2004. Strong directivity of ocean-generated seismic noise, *Geochem. Geophys. Geosyst.,* **5,** Q03004, doi:10.1029/2003GC000520.

Sens-Schonfelder, C. & Wegler, U., 2006. Passive image interferometry and seasonal variations of seismic velocities at Merapi volcano, Indonesia, *Geophys. Res. Lett.,* **33,** L21302, doi:10.1029/2006GL027797.

Shapiro, N. & Campillo, M., 2004. Emergence of broadband rayleigh waves from correlations of the ambient seismic noise, *Geophys. Res. Lett.,* **31,** L07614, doi:10.1029/2004GL019491.

Shapiro, N., Campillo, M., Stehly, L. & Ritzwoller, M., 2005. High resolution surface wave tomography from ambient seismic noise, *Science,* **307,** 1615–1618.

Stehly, L., Campillo, M. & Shapiro, N., 2006. A study of the noise from its long-range correlation properties, *J. geophys. Res.,* **111,** B10306, doi:10.1029/2005JB004237.

Stutzmann, E., Roult, G. & Astiz, L., 2000. Geoscope station noise level, *Bull. seism. Soc. Am.,* **90**(3), 690–701.

Stutzmann, E. et al., 2001. Moise: a prototype multi-parameter ocean bottom station, *Bull. seism. Soc. Am.,* **91**(4), 885–892.

Stutzmann, E., Schimmel, M., Patau, G. & Maggi, A., 2009. Global climate imprint on seismic noise, *Geochem. Geophys. Geosyst.,* **10,** Q11004, doi:10.1029/2009GC002619.

Tolman, H., 1991. A third generation model for wind on slowly varying, unsteady and inhomogeneous depth and currents, *J. Phys. Oceanogr.,* **21,** 766–781.

Tolman, H., 2008. A mosaic approach to wind wave modeling, *Ocean Model.,* **25,** 35–47.

Tournadre, J., Whitmer, K. & Girard-Ardhuin, F., 2008. Iceberg detection in open water by altimeter waveform analysis, *J. geophys. Res.,* **117**(7), C08040, doi:10.1029/2007JC004587.

Tsai, V., 2009. On establishing the accuracy of noise tomography travel-time measurements in a realistic medium, *Geophys. J. Int.,* **178,** 1555–1564 doi: 10.1111/j.1365-246X.2009.04239.x.

Tsai, V. & McNamara, D., 2011. Quantifying the influence of sea ice on ocean microseism using observations from the bering sea, Alaska, *Geophys. Res. Lett.,* **38,** L22502, doi:10.1029/2011GL049791.

Webb, S., 1992. The equilibrium oceanic microseism spectrum, *J. acoust. Soc. Am.,* **92,** 2141–2158, doi:10.1121/1.405226.

Webb, S., 1998. Broadband seismology and noise under the ocean, *Rev. Geophys.,* **36,** 105–142.

Webb, S. & S.C., C., 1986. Microseism propagation between two sites on the deep seafloor, *Bull. seism. Soc. Am.,* **76,** 1433–1445.

Wegler, U. & Sens-Schonfelder, C., 2007. Fault zone monitoring with passive image interferometry, *Geophys. J. Int.,* **168,** 1029–1033, doi:10.1111/j.1365-246X.2006.03284.x.

Yang, Y. & Ritzwoller, M., 2008. The characteristics of ambient seismic noise as a source for surface wave tomography, *Geochem. Geophys. Geosyst.,* **9**(2), Q02008, doi 10.1029/2007GC001814.